Electronic Supplementary Information

Ultrathin Paper-like Boron-doped Carbon Nanosheet Electrodes Combined with Boron-enriched Gel Polymer Electrolyte for High-Performance Energy Storage

Chuanlin Cai,[a‡] Ping Yuan,[a‡] Jiayong Tang,[a] Yanhui Guo,*[a,b] Xiaohua Ma*[a]

[a]Department of Materials Science, Fudan University, 200433, Shanghai, China.

[b]Inorganic Chemistry Laboratory, Department of Chemistry, University of Oxford, South Parks Road, Oxford, OX1 3QR, UK.

E-mail: xhma@fudan.edu.cn; yanhui.guo@chem.ox.ac.uk

‡ These authors contributed equally to the work.

Fig. S1 (a) GO dispersion (2 mg ml^{-1}) in anhydrous tetrahydrofuran (left) and reduced boron-doped graphene colloid after treatment with lithium borohydrides (right). (b-d) The highly flexible and mechanically robust nature of the as-prepared ultrathin boron-doped graphene paper.

Fig. S2 Top view SEM image of the as-prepared (a) B-GP-1, (b) B-GP-3 and (c) B-GP-5.

Fig. S3 XRD spectrum of B-GP-1, B-GP-3 and B-GP-5.

Fig. S4 (a) TEM image of the as-prepared B-GP-3. (b) The selected area electron diffraction (SAED) pattern of B-GP-3. (c) Dark-field STEM image of B-GP-3 with the corresponding elemental mapping images.

Fig. S5 (a-b) FT-IR spectra and (c) Raman spectra of B-GP-1 and B-GP-5. (d) Survey-scan XPS spectra of GO and B-GP-3.

Table S1 Elemental analyses results of B-GP-3.

Fig. S6 (a) Synthesis route of homopolymer P(GMMA-PBA). (b-c) The SEM images of the P(GMMA-PBA).

Fig. S7 The comparison of GCD tests with various current densities within the potential window of 0~2.5 V for (a) B-GP-1, (b) B-GP-3 and (c) B-GP-5 electrodes assembled in a symmetrical capacitors using the electrochemical working station of CHI 660E. The thickness of each electrodes and the total mass of electrodes for three different symmetrical capacitors keep the same.

Fig. S8 Various lasting time of two red LED lamps using one fully charged symmetrical capacitor at current density of 1 A g^{-1} within the potential window of 0~2.5 V. Graphs (a~d) present the different lasting time of 5 s, 60 s, 120 s, and 180 s, respectively.

Fig. S9 Equivalent circuit for the symmetric supercapacitor.

Table S2 Impedance data obtained from Nyquist plots by fitting to an equivalent electrical circuit in Fig. S8

Table S3 EIS result of some typical works with GPE used.

Table S4 EIS analyses of some typical works with organic or aqueous electrolytes.

Fig. S10 Comparison of EIS spectra of the all-solid-state flexible SC fabricated with B-GP-1 and B-GP-3 electrodes.

Reference

1 O. C. Compton, S. T. Nguyen, *Small* 2010, **6,** 711.

2 M. Enterría, M. F. R. Pereira, J. I. Martins, J. L. Figueiredo, *Carbon* 2015, **95,** 72.

3 F. Xiao, S. X. Yang, Z. Y. Zhang, H. F. Liu, J. W. Xiao, L. Wan, J. Luo, S. Wang and Y. Q. Liu, *Sci Rep*, 2015, **5,** 8.

4 K. Chi, Z. Y. Zhang, J. B. Xi, Y. A. Huang, F. Xiao, S. Wang and Y. Q. Liu, *Acs Applied Materials & Interfaces*, 2014, **6,** 16312-16319.

5 G. Wang, X. Sun, F. Lu, H. Sun, M. Yu, W. Jiang, C. Liu and J. Lian, *Small*, 2012, **8,** 452-459.

6 M. Endo, C. Kim, K. Nishimura, T. Fujino and K. Miyashita, *Carbon,* 2000, **38,** 183-197.

7 C. Li, Y. Hu, M. H. Yu, Z. F. Wang, W. X. Zhao, P. Liu, Y. X. Tong, X. H. Lu, *Rsc Adv.* 2014, **4,** 51878.

8 R. Ramachandran, M. Saranya, V. Velmurugan, B. P. C. Raghupathy, S. K. Jeong, A. N. Grace, *Appl. Energy* 2015, **153,** 22.

9 K. Han, J. Shen, S. Hao, H. Ye, C. Wolverton, M. C. Kung, H. H. Kung, *ChemSusChem* 2014, **7,** 2545.

10 P. Yuan, C. Cai, J. Tang, Y. Qin, M. Jin, Y. Fu, Z. Li and X. Ma, *Advanced Functional Materials,* 2016, **26,** 5930-5939.

11 J. Tang, M. Jin, P. Yuan, Y. Fu and X. Ma, *Advanced Energy Materials,* 2016, **6,** 1600146.

12 M. J. Jiang, J. D. Zhu, C. Chen, Y. Lu, Y. Q. Ge and X. W. Zhang, *Acs Applied Materials & Interfaces*, 2016, **8,** 3473-3481.

13 Z. Wang, D. Mo, X. Ma, J. Xu, W. Zhou, Q. Jiang, Z. Feng, J. Xiong, D. Zhu and Q. Zhou, *Electrochimica Acta,* 2015, **184,** 338-346.

14 Y. Kumar, G. P. Pandey and S. A. Hashmi, *J. Phys. Chem. C,* 2012, **116,** 26118-26127.

15. T. Sato, S. Marukane, T. Morinaga, T. Kamijo, H. Arafune and Y. Tsujii, *Journal of Power Sources*, 2015, **295**, 108-116.

16 J. Li, X. Zhang, R. Peng, Y. Huang, L. Guo and Y. Qi, *RSC Advances*, 2016, **6**, 54866-54873.

17 Y. Zhang, C. Zhang, G. Huang, B. Xing and Y. Duan, *Electrochimica Acta*, 2015, **166**, 107-116.

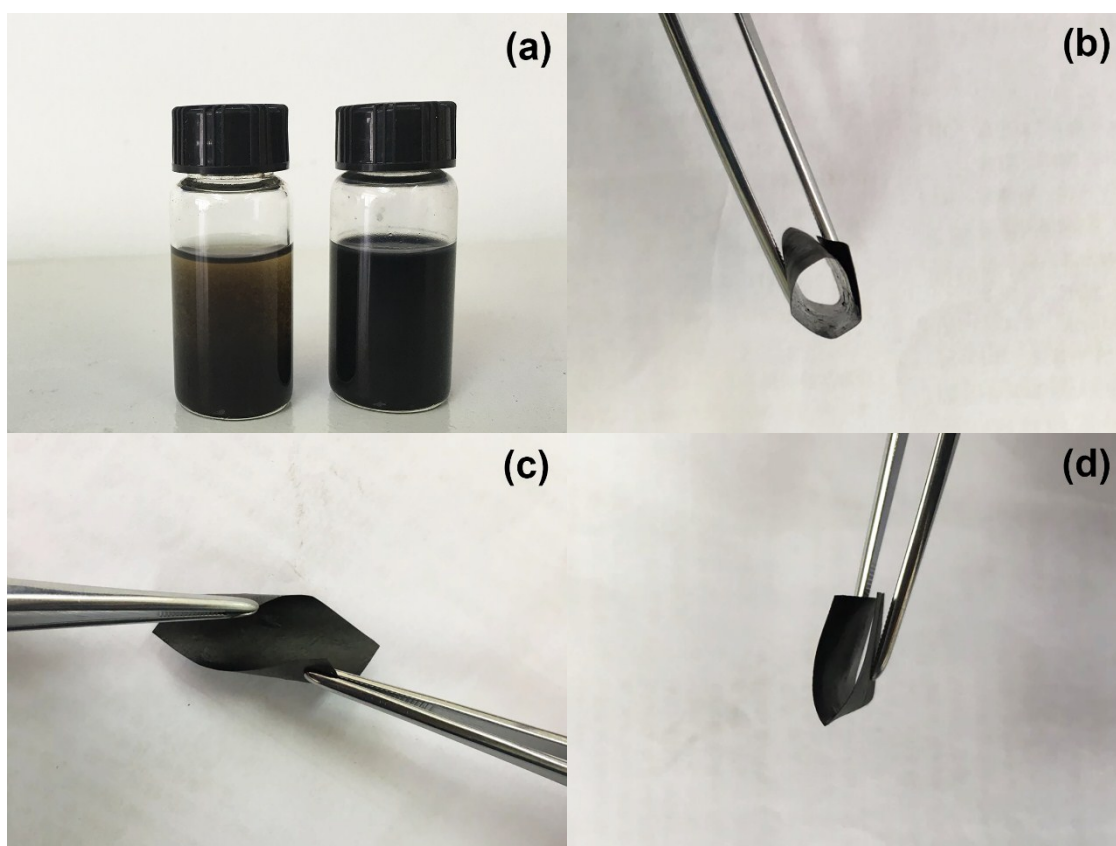18 D. Bhattacharjya and J.-S. Yu, *Journal of Power Sources*, 2014, **262**, 224-231.

Fig. S1 (a) GO dispersion (2 mg ml^{-1}) in anhydrous tetrahydrofuran (left) and reduced boron-doped graphene colloid after treatment with lithium borohydrides (right). (b-d) The highly flexible and mechanically robust nature of the as-prepared ultrathin boron-doped graphene paper.
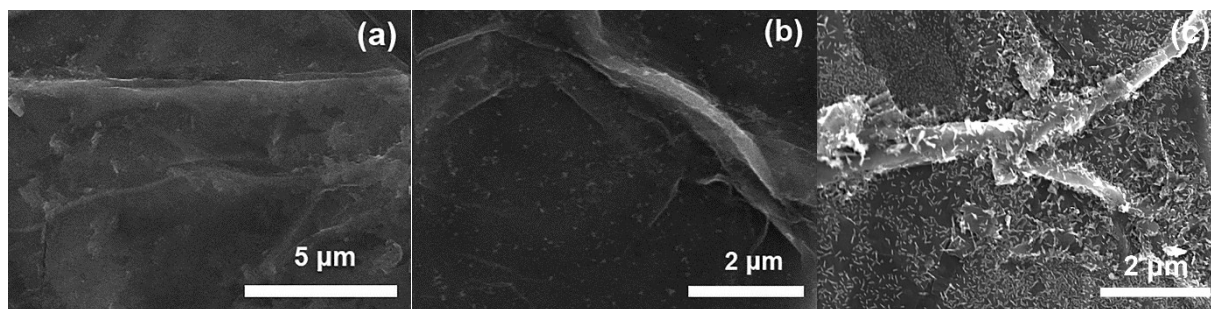
Fig. S2 Top view SEM image of the as-prepared (a) B-GP-1, (b) B-GP-3 and (c) B-GP-5.

Increasing the mass ratio of lithium borohydrides to graphene oxide, the reduction and doping degree are gradually raised. The B-GP-3 paper shows more wrinkles than B-GP-1, suggesting higher degree of reduction and doping.[1] Meanwhile, little amount of nanostructured borates are homogeneously distributed on the graphene layers. However, large amount of borates particles are aggregated on the graphene sheets of B-GP-5, which hinder the contact of the electrolyte with active materials and the charge transfer during charging/discharging process.[2]
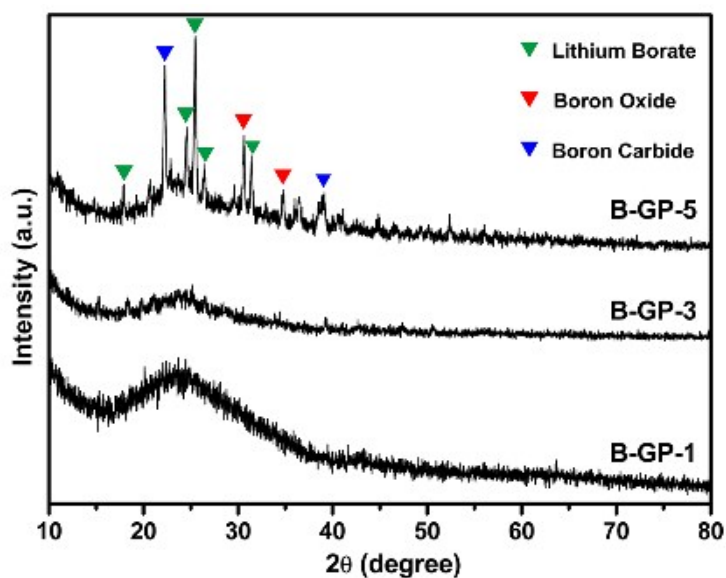
Fig. S3 XRD spectrum of B-GP-1, B-GP-3 and B-GP-5.

As shown in Figure S3, a broad peak centering at 2θ = 24° for the graphite (002) plane arises for all of three B-dope graphene papers, proving the efficient reduction of GO via the lithium borohydride.[3-4] In addition, the intensity of the broad peak decreased gradually, indicating that the distance between B-doped carbon nanosheets were enlarged and the formation of loose and porous structure.[5] Some peaks assigned to lithium borate and boron carbide appear on B-GP-5, which may account for the decreased comprehensive properties.[6]
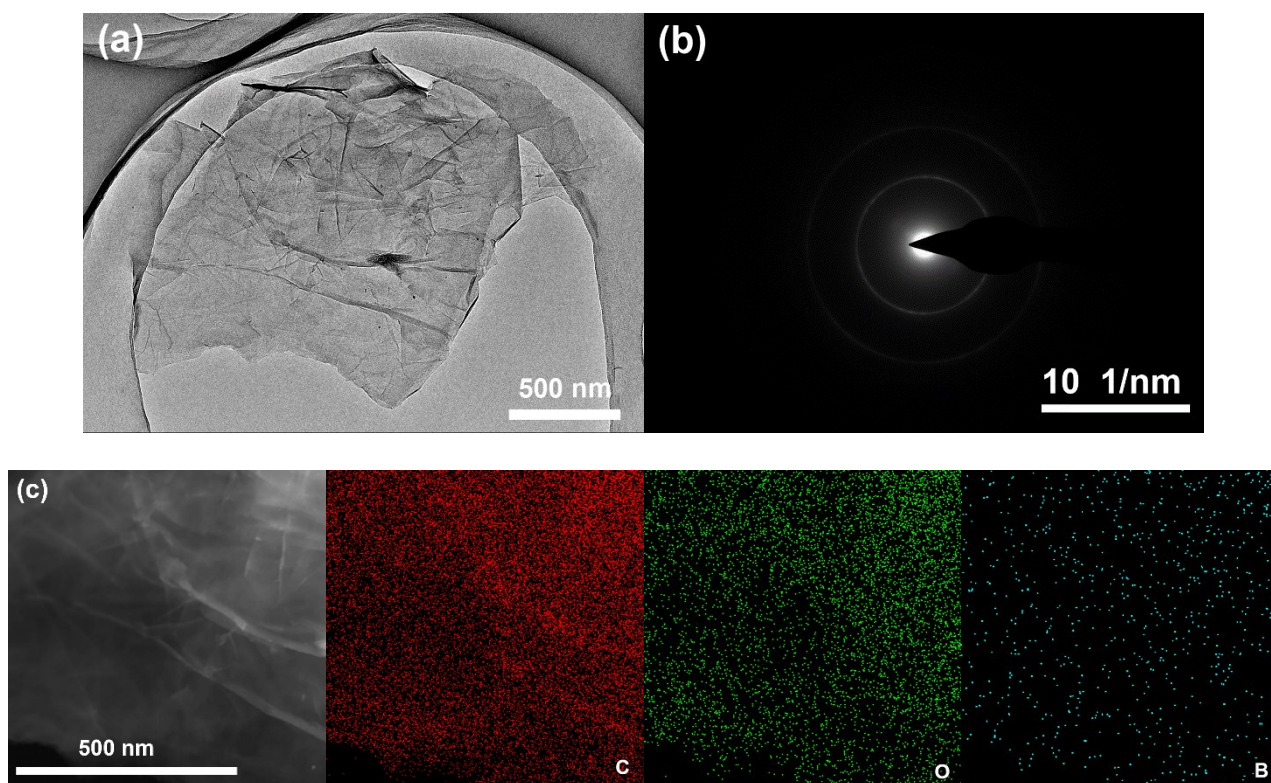
Fig. S4 (a) TEM image of the as-prepared B-GP-3. (b) The selected area electron diffraction (SAED) pattern of B-GP-3. (c) Dark-field STEM image of B-GP-3 with the corresponding elemental mapping images.

Figure S4a presents the TEM image of B-GP-3, of which the low contrast image indicates only very few layers of graphite sheets constructs the graphene layer.[7] The dim SAED pattern (Figure S4b) reveals that the B-GP-3 is not well crystallized. Dark-field STEM images and the corresponding elemental mapping images of C, O, and B are shown in Figure S4c. The boron is well-distributed in the graphene matrix.
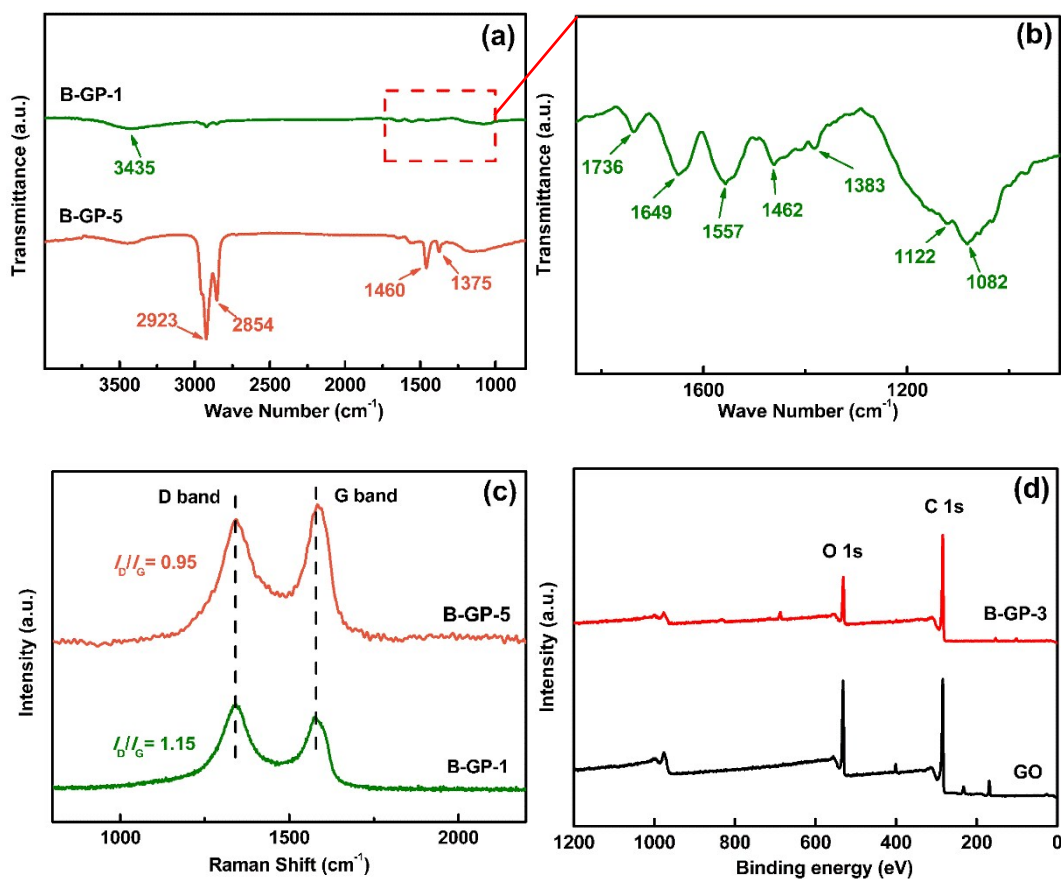
Fig. S5 (a-b) FT-IR spectra and (c) Raman spectra of B-GP-1 and B-GP-5. (d) Survey-scan XPS spectra of GO and B-GP-3.

Raman: The spectrum of graphene is characterized by two prominent peaks such as G and D band. The G band is due to the first order Raman scattering of the E2g phonon of sp^2 carbon domains, while D band is from the breathing mode of k-point phonons of A1g attributed to the graphene edges.[8] The value of I_D/I_G of B-GP samples varies from 1.15 (B-GP-1), 1.17 (B-GP-3) to 0.95 (B-GP-5), which also confirms that the oxygenated groups have been removed during the reduction process. In addition, I_D/I_G values can be attributed to the higher densities of structural defects and disorder consequent of doping, which prove the highest doping degree of B-GP-3 among the as-prepared materials.[9]

Table S1 Elemental analyses results of B-GP-3

Sample	C [atomic%]	O [atomic%]	N [atomic%]	B [atomic%]
GO	70.08	29.92	-	-
B-GP-3	82.59	16.07	0.63	0.70

XPS: Elemental analysis have been well investigated by X-ray photoelectron spectroscopy (XPS). Comparison of XPS survey spectra of GO and B-GP-3 samples shows a dramatic diminishment in oxygen peaks after reduction, indicating the removal of oxygen functional groups (Fig. S4d). Table S1 based on XPS spectra shows the $LiBH_4$ reduction in anhydrous THF greatly increased the C/O atomic ratio from 2.34 to 5.14.
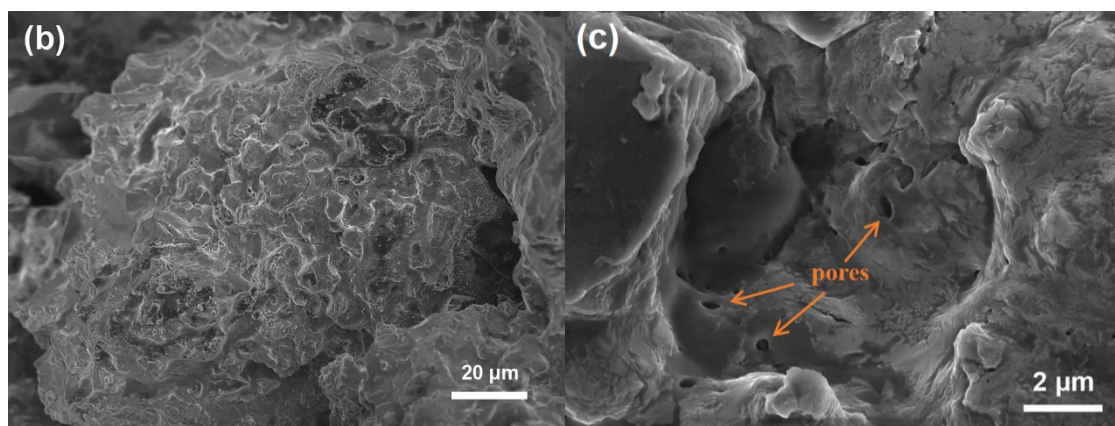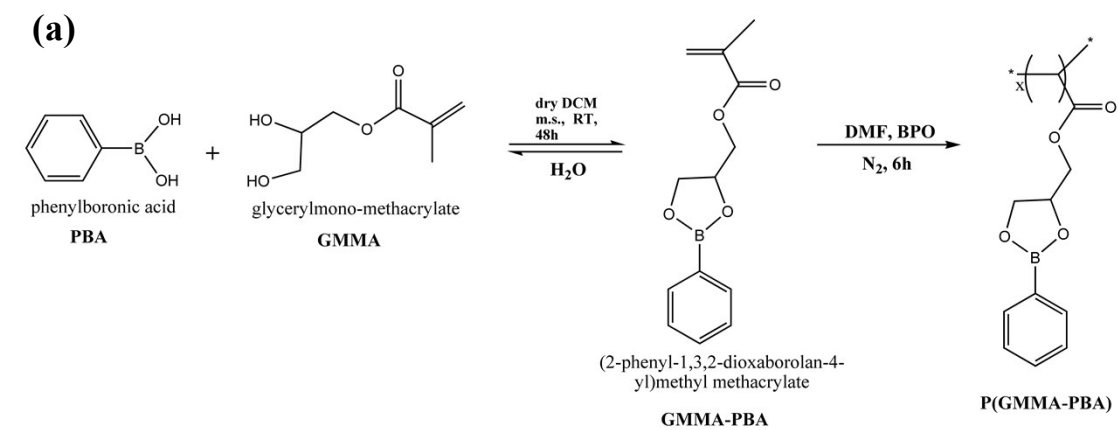
Fig. S6 (a) Synthesis route of homopolymer P(GMMA-PBA). (b-c) The SEM images of the P(GMMA-PBA).
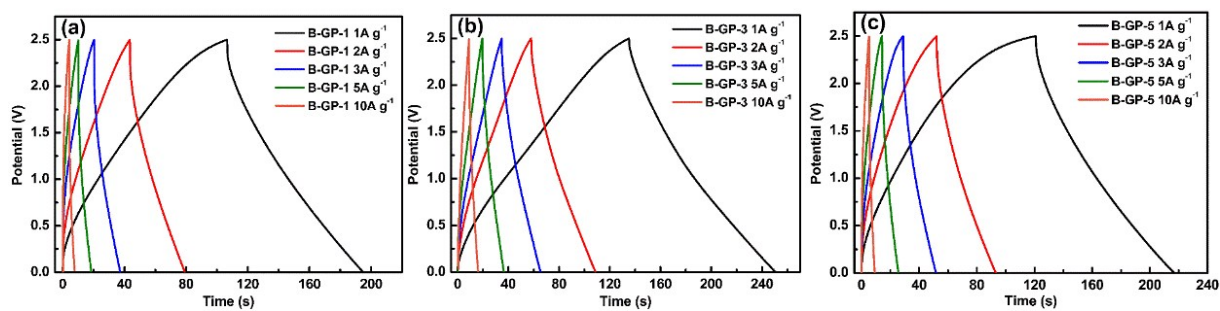
Fig. S7 The comparison of GCD tests with various current densities within the potential window of 0~2.5 V for (a) B-GP-1, (b) B-GP-3 and (c) B-GP-5 electrodes assembled in a symmetrical capacitors using the electrochemical working station of CHI 660E. The thickness of each electrodes and the total mass of electrodes for three different symmetrical capacitors keep the same.
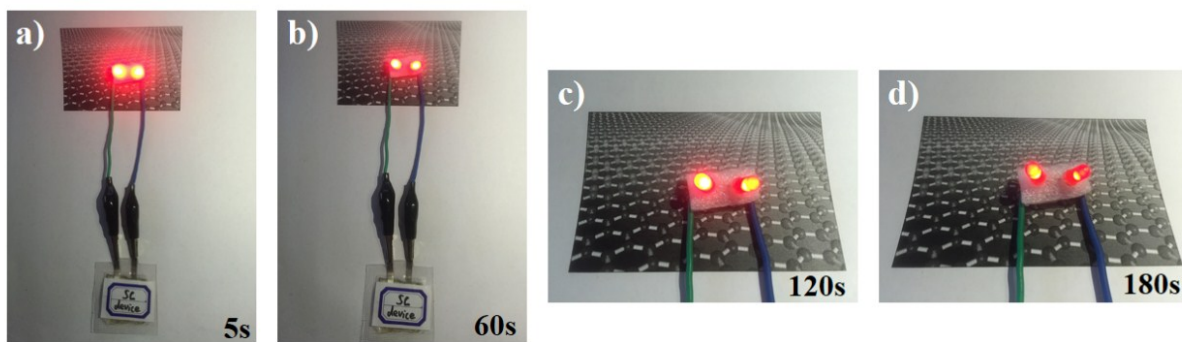
Fig. S8 Various lasting time of two red LED lamps using one fully charged symmetrical capacitor at current density of 1 A g^{-1} within the potential window of 0~2.5 V. Graphs (a~d) present the different lasting time of 5 s, 60 s, 120 s, and 180 s, respectively.
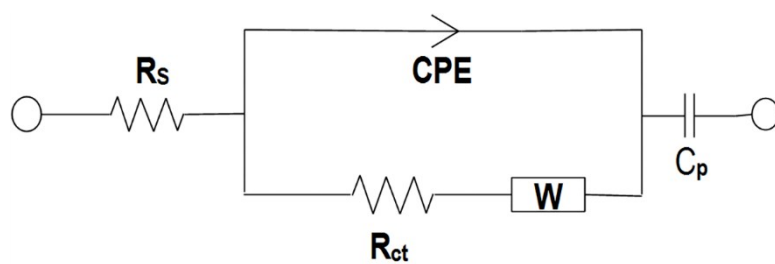
Fig. S9 Equivalent circuit for the symmetric supercapacitor.

Table S2 Impedance data obtained from Nyquist plots by fitting to an equivalent electrical circuit in

Fig. S9

Samples B-GP-3	R_s (Ω)	R_{ct} (Ω)	Z_w
Before cycling test	12.390	0.270	0.001
After cycling test	13.680	0.277	0.001

Table S3 EIS analyses of some typical works with GPE used.

Materials	Electrolytes	R_s (Ω)	R_{ct} (Ω)	Ref.
rGO	GPE	21.15	5.65	**10**
rGO	GPE	14.12	1.28	**11**
G-MFO	GPE	15.08	1.73	**11**
G-MoS2	GPE	14.46	1.45	**11**
AC	PVAPB GPE	0.54	0.22	**12**
PEOTT-b	ACN–LiClO$_4$	58.7	3.70	**13**
AC	ILGPE-1	6.8	4.5	**14**
AC	ILGPE-2	5.3	3.0	**14**
B-GP	GPE	12.39	0.27	**This work**

As shown in Table S3, the R_s of the symmetrical capacitor is 12.39 Ω, and the corresponding R_{ct} is 0.27 Ω. It can be deduced that the rich micropores and the unique structure enlarges the inter-layer spacing between the B-doped carbon nanosheets, providing a shortened diffusion path for electron transport and allowing ions in the electrolyte to easily penetrate through the sheets (Figure 2d). According to our previous works and other researchers' reports, it remains reasonable when the R_s is greater than R_{ct}, especially for the gel polymer electrolyte system used in this work. It may lead to a much smaller R_{ct} than other electrolyte system.

Table S4 EIS analyses of some typical works with organic or aqueous electrolytes.

Materials	Electrolytes	R_s (Ω)	R_{ct} (Ω)	Ref.
AC	DEME-TFSI/PC	0.34	1.97	**15**
AC	DEME-TFSI	0.95	1.99	**15**
LMO/AC	$LiPF_6$/EC:DEC:DMC	4.90	15.50	**16**
LMO-MSs/AC	$LiPF_6$/EC:DEC:DMC	2.42	30.20	**16**
HPCs-MnO_2-52	KOH	0.18	2.56	**17**
ACDC-1	Et_4NBF_4/AN	0.94	6.94	**18**
ACDC-3	Et_4NBF_4/AN	0.81	10.52	**18**

Furthermore, we have also compared with other cell systems with organic or aqueous electrolytes. T. Sato et al. have investigated the effect of different electrolytes on electrochemical performances by fabricating the capacitor cell with conventional organic liquid, neat ion liquid (IL) and solid polymer electrolyte.[15] The EIS results demonstrated that a small R_{ct} is a major feature of solid electrolyte system and the R_s of the cell could be reduced by reducing the thickness of the polymer electrolyte film. Based on the analyses above, we can prove that in this manuscript the B-contained GPE membrane (P(GMMA-PBA)) as electrolyte lead to a higher R_s value.
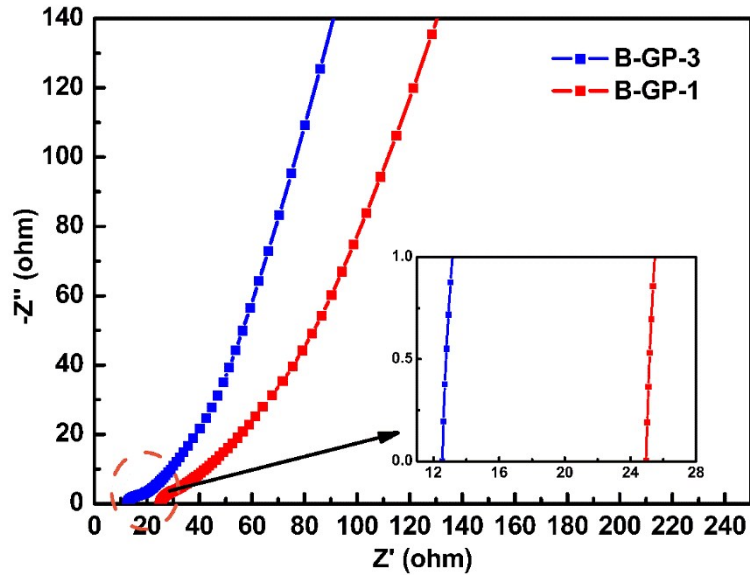
Fig. S10 Comparison of EIS spectra of the all-solid-state flexible SC fabricated with B-GP-1 and B-GP-3 electrodes.

Fig. S10 shows the comparison of EIS spectra of the flexible SC fabricated with B-GP-1 and B-GP-3 electrodes. As we all know, the equations between the internal resistance and conductivity are as follows:

$$R = \rho \frac{l}{s} \tag{1}$$

$$\sigma = \frac{1}{\rho} \tag{2}$$

Where R is the internal resistance, ρ is the resistivity, l is the length of the material, s is the sectional area, and σ is the conductivity.

The intercept at high frequency on the real axis is the intrinsic internal resistance (R_s) of the electrode material and electrolyte of device. As shown in **Fig. S10**, we notice that the R_s of B-GP-1 (24.89 Ω) is much higher than that of B-GP-3 (12.39 Ω). In this work, all the EIS experiment are conducted with the same B-contained GPE membrane (P(GMMA-PBA)), except the different electrode material (B-GP-1 and B-GP-3). The electrode material with higher value of R_s suggest that it possesses a higher value of resistivity, in other words, a lower conductivity.

Furthermore, the electronic properties of B-GP-1 and B-GP-3 are apparently different. Since the larger amount of lithium borohydrides was used in preparation of B-GP-3, it means that the reduction degree of B-GP-3 is much higher than that of B-GP-1. Restoring the honeycomb structure of sp^2-bonded carbon network in the reduction process can increase the conductivity. Meanwhile, all the CV and GCD tests in manuscript also declare that the electrochemical performance is better for B-GP-3. And the electrochemical performance can also reflect the conductivity of electrode materials to some extent.